Spin-State dependent Conductance Switching in Single Molecule-Graphene Junctions

Enrique Burzurí,[*,†,‡] Amador García-Fuente,[¶] Victor García-Suárez,[¶] Kuppusamy Senthil Kumar,[§,‖] Mario Ruben,[§,‖] Jaime Ferrer,[*,¶] and Herre S. J. van der Zant[†,⊥,#]

†*Kavli Institute of Nanoscience, Delft University of Technology, PO Box 5046, 2600 GA Delft, The Netherlands*

‡*IMDEA Nanoscience, Ciudad Universitaria de Cantoblanco, C/Faraday 9, 28049 Madrid, Spain*

¶*Departamento de Física, Universidad de Oviedo and CINN (CSIC), ES-33007 Oviedo, Spain*

§*Institut of Nanotechnology, Karlsruhe Institut of Technology (KIT), D-76344 Eggenstein-Leopoldshafen, Germany*

‖*Institute de Physique et Chimie de Materiaux de Strasbourg (IPCMS), UMR 7504, CNRS-Universite de Strasbourg, F-67034 Strasbourg, France*

⊥*IMDEA Nanoscience, Ciudad Universitaria de Cantoblanco, c/Faraday 9, 28049 Madrid, Spain*

#*Departamento de Física de la Materia Condensada and Condensed Matter Physics Center (IFIMAC), Universidad Autónoma de Madrid, E-28049 Madrid, Spain*

E-mail: e.burzurilinares@tudelft.nl; j.ferrer@cinn.es

Abstract

Spin-crossover (SCO) molecules are versatile magnetic switches with applications in molecular electronics and spintronics. Downscaling devices to the single-molecule level remains, however, a challenging task since the switching mechanism in bulk is mediated by cooperative intermolecular interactions. Here, we report on electron transport through individual Fe-SCO molecules coupled to few-layer graphene electrodes *via* $\pi-\pi$ stacking. We observe a distinct bistability in the conductance of the molecule and a careful comparison with density functional theory (DFT) calculations allows to associate the bistability with a SCO-induced orbital reconfiguration of the molecule. We find long spin-state lifetimes that are caused by the specific coordination of the magnetic core and the absence of intermolecular interactions according to our calculations. In contrast with bulk samples, the SCO transition is not triggered by temperature but induced by small perturbations in the molecule at any temperature. We propose plausible mechanisms that could trigger the SCO at the single molecule level.

Keywords

spin-crossover (SCO), molecular spintronics, graphene electrodes, density functional theory (DFT), magnetic switch

Tuning the magnetic properties of individual molecules is sought in molecular spintronics as the key to fabricate switchable molecule-scale electronic components.[1–3] The tuning mechanisms in spin-crossover (SCO) complexes are particularly versatile.[4–7] The spin value of the molecular magnetic core, typically an Fe(II) complex, can be switched between a high-spin (HS) and a low-spin (LS) state by modifying its local geometry with light,[8,9] pressure,[10,11] temperature,[12,13] voltage[14] or the adsorption of molecules.[15–17] SCO switching with temperature is well established in macroscopic crystals where the molecular geometry is well defined and stable in an ordered lattice. The change in spin state can be detected for example as a change in the crystal color[17] or the magnetic susceptibility.[12] Additionally, the electrical current has been used as a probe for the spin state switching in thin films of nanoparticles[13,18]

and molecular thin films.[19]

Downscaling to the single-molecule level, however, entails a fundamental difference[20] with respect to measurements on large assemblies: the cooperative intermolecular interactions that mediate the SCO in e.g. crystals[21,22] are absent. To overcome this, alternative strategies based on porphyrin, terpyridine and bispyridine derivatives have recently been developed. The SCO is now induced at the molecular level by either electrostatic effects[14,23] or molecular stretching[24,25] in a single-molecule break-junction. The current through the molecule then acts as the tool to detect the SCO transition where bulk characterization methods fail. At present, it is however still unclear what happens for individual molecules that show a temperature-induced SCO transition but are now embedded in a solid-state device where the steric hindrance felt by the molecule in the crystal is absent. Structural distortions induced in single molecules by their contacts to metallic (Au) surfaces or electrodes are well known to modify their magnetism[26–29] and even quench the SCO mechanism.[30]

Graphene electrodes are crucial to study individual temperature-induced SCO molecules. They have proved to be stable from cryogenic up to room temperatures[31] in contrast to gold nanoelectrodes, enabling the study of temperature-induced SCO transitions in single molecules around room temperature. In addition, a soft molecule-graphene coupling *via* $\pi-\pi$ stacking may contribute to preserve the electronic structure of the molecular orbitals[32] while providing the flexibility to allow for the SCO transition to occur, as demonstrated for molecules on HOPG surfaces.[33]

In this work we study electron transport through individual Fe-based SCO molecules linked *via* $\pi-\pi$ stacking to nanometer-spaced few-layer graphene (FLG) electrodes. We observe a reproducible conductance bi-stability between two well-defined states - a strong indication that the spin-crossover switch is active in our single-molecule junctions. In contrast with the temperature-induced transition observed in macroscopic crystals of these molecules, the SCO behavior at the single-molecule level is not triggered at any specific temperature. The reproducibility of the main conductance characteristics has allowed us to carry a careful

comparison with calculations. Density functional theory (DFT) simulations show that the SCO transition induces a sharp change in the energy spectrum of the molecular orbitals close enough to the Fermi level to be relevant for the electronic transport properties on the junctions. This result translates into a conductance bi-stability, in excellent agreement with the experiments. We find that small perturbations (2.5 %) of the distance between the Fe(II) ion and its coordinated ligand atoms can trigger the switch between the HS and LS states. Interestingly, the DFT simulations predict that the high-spin transmission is spin-resolved up to relatively high energies.

We use an $[Fe(\mathbf{L})_2](BF_4)_2{\cdot}CH_3CN{\cdot}H_2O$ molecule,[12] hereafter referred to as Fe-SCO, where **L** is the ligand 4-(2,6-di(1*H*-pyrazol-1-yl)pyridin-4-yl)benzyl-4-(pyren-1-yl)butanoate. A schematic cartoon of this molecule is shown in Figure 1(a). The Fe(II) ion is coordinated with two 2,6-bispyrazolylpyridine (bpp) ligands in an octahedral (O_h) symmetry distorted to a S_4 symmetry because of the ligand-Fe(II) coordination specific to this molecule. In addition, our DFT calculations show that the molecule undergoes a Jahn-Teller distortion that reduces the symmetry even further (see Section 3 in the Supplemental Material). The extended backbone is made of two benzoyl ester and C_3 alkyl groups symmetrically connected to the bpp units, thus providing extra length and flexibility to the molecule. These ligands are connected to two pyrene ending-groups that promote soft anchoring to graphene *via* $\pi - \pi$ stacking. Additional details on the molecule and its synthesis can be found in Ref.[12]

The ligand field interaction of approximate O_h symmetry felt by the Fe(II) ion splits the 5-fold degenerate energy spectrum of its $3d$ electronic shell into two well separated e_g and t_{2g} levels by a ligand field splitting energy Δ as shown schematically in Figure 1(c). Δ depends on the average distance r between the central Fe(II) ion and its neighboring ligand atoms approximately as r^{-5},[34] and therefore depends inversely on temperature due to the thermal expansion effect. At low temperatures Δ is larger than the exchange interaction J among the six d electrons in the Fe(II) ion. As a result, the Fe-SCO molecules are in a low-spin (LS)

$S = 0$ ground state (see Figure 1(c)). However, Δ decreases with increasing temperature because of thermal expansion and becomes eventually smaller than J as the temperature is raised, making the e_g states accessible. These levels are then filled to maximize the spin according to Hund's first principle, resulting in a high-spin (HS) state $S = 2$ above a certain temperature (see Figure 1(c)). The magnetic characterization of crystals (bulk) made of these Fe-SCO molecules shows that the spin-crossover transition between HS and LS states occurs at around $T_c = 225$ K.[12] Interestingly, it is already observed in crystals made of Fe-SCO molecules that structural factors, such as the length or flexibility of the molecule, are determinant to trigger or not the spin-crossover transition.[12]

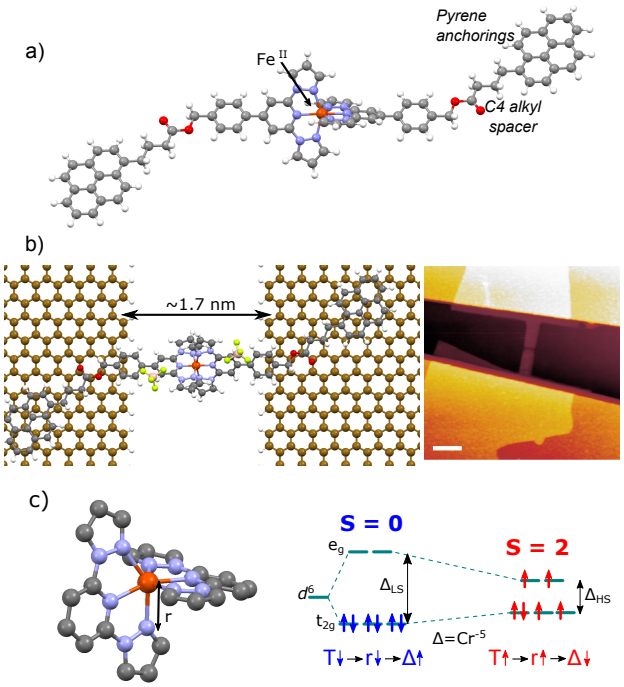

Figure 1: The spin-crossover-FLG single-molecule junction. (a) Molecular structure of the Fe-SCO molecule: an Fe(II) ion is coordinated with two 2,6-bispyrazolylpyridine (bpp) ligands in a distorted octahedral symmetry. Two benzoyl ester and C_3 alkyl groups symmetrically connected to the bpp units serve as the backbone of the molecule. Additionally, two pyrene ending-groups provide a soft anchoring to graphene *via* $\pi - \pi$ stacking. BF_4^- counter anions are omitted for clarity. (b) Schematics and AFM image of a graphene/Fe-SCO/graphene single-molecule junction. Color code: C grey, O red, Fe orange, N lilac, F yellow, B pink, H white. The scale bar is 500 nm. (c) Mechanism of the SCO transition in crystals of Fe-SCO molecules: a change in the Fe-N ligand distance r induced by temperature modifies the crystal field splitting Δ. The different filling of the orbitals leads to a change in the ground state spin from $S = 0$ to $S = 2$.

In our devices, a single Fe-SCO molecule is anchored to two FLG electrodes. A schematic representation of the FLG/Fe-SCO/FLG junction and an atomic force microscopy (AFM) image is shown in Figure 1(b). FLG flakes are deposited on a Si/SiO_2 substrate by mechanical exfoliation. Thereafter, a nanometer-size gap between source and drain is fabricated by electroburning[31,35] of 100-200 nm-wide pre-patterned bridges in the flakes[36] that are narrowed down during electroburning. See additional details in Section 1.1 of the Supplemental Material. Typical gap sizes after electroburning range[37] in the order of 1-2 nm while the length of the molecule spans over 4 nm, so that a substantial part of the molecular backbone may also be lying on the FLG electrodes as depicted in Figure 1(b). The advantage of this configuration is that the anchoring groups lie farther from the edges, facilitating the coupling to graphene by $\pi-\pi$ stacking.[37] In this paper, including the Supplemental Material, we discuss six molecular junctions that show molecular features and together they provide a consistent set of data.

Figure 2(a-c) shows the current (I) - voltage (V) characteristics measured at cryogenic temperatures in three different junctions after deposition of the Fe-SCO molecules. When compared with the empty junction, a sharp increase in the current of around two orders of magnitude indicates the formation of a molecular junction (see Section 1.2 in the Supplemental Material). In all these junctions, a clear bi-stability appears between two well-defined states: a large-gap (LG) state (blue curve) and a small-gap (SG) state (red curve). The low-bias current is strongly suppressed in both states. This is a signature of off-resonant transport in a Coulomb blockade regime. At higher bias, sharp resonances at threshold voltages $V_{\mathrm{SG}} \approx 0.1$-$0.2$ V in the SG state and $V_{\mathrm{LG}} \approx 0.5$ V in the LG state lift the conductance blockade revealing resonant transport through a molecular orbital with the $V_{\mathrm{LG,SG}}$ being twice the distance to the closest molecular orbital when expressed in energy.[38] These blockade and resonant transport features are more clearly seen in the differential conductance $\mathrm{d}I/\mathrm{d}V$ curves shown in Figure 2(d). Sample 5 with a similar bistable behavior is shown in the Supplemental Material. An additional sample (sample 4) that does not show

a bi-stability appears to be "trapped" in the SG state with similar resonant voltages (see Section 2 in the Supplemental Material). The source of the negative differential resistance observed in samples 3 and 5 could be found in the intrinsic functionalities of some graphene edges' shapes[39] (see Section 2.1 of the Supplemental Material.)

Bistable conductance characteristics have been observed for SCO nanoparticles[13,35] and electrically[14] or mechanically[24] induced SCO molecules coupled to gold electrodes. The sharp change in the resonant voltage from V_{SG} to V_{LG} in our junctions is indicative of an abrupt change in the molecular orbitals around the Fermi level of graphene, tentatively induced by the SCO transition. We further note that current levels and the resonant voltage are reproducible from junction to junction for both LG and SG states. This reproducibility could stem from the electrode-molecule anchoring geometry facilitated by graphene, as seen in other reports[37,40–42] and predicted in theoretical simulations.[32]

Hereafter, we discuss the stability of the SG and LG states as a function of temperature and time. Figure 3(a) shows a representative color plot of I measured as a function of V while decreasing the temperature in sample 3. A telegraph-like switch is observed between well-separated states. Note, that this kind of time-dependent switch has not been observed in empty graphene junctions nor in junctions containing molecules coupled to graphene *via* π-π but without SCO functionality[36,37,40,41] and that the current levels are orders of magnitude below those observed in electroburned graphene junctions of carbon chains,[43] as expected in molecular junctions. In contrast to crystals of these molecules, the switching mechanism appears not to be triggered at a specific temperature and persists well below the bulk HS-LS transition temperature. This is *a priori* not surprising since the steric hindrance in the crystal is different than that for a single molecule and the SCO transition may sensitively depend on the local geometry adopted by the molecule in the junction.[24]

Figure 3(b) shows a current *versus* time trace measured during 10 seconds at a fixed bias voltage of -0.6 V and at 4 K. The voltage is larger than V_{SG} and lower than V_{LG}, and T is set well below the SCO transition temperature reported for crystals. The area enclosed in

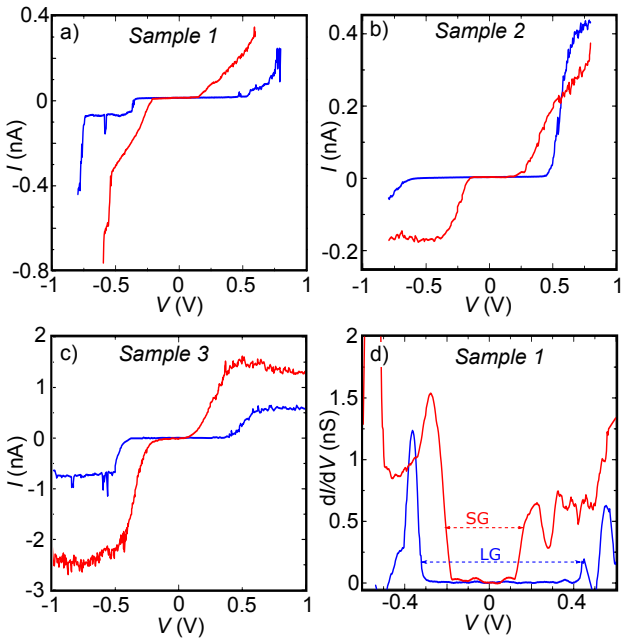

Figure 2: Spin-crossover bistable current-voltage characteristics. (a-c) Current-voltage characteristics measured at $T = 4$ K in three different junctions containing an Fe-SCO molecule. A clear bi-stability between a small gap (SG, red) and large gap (LG, blue) states is observed. The low-bias current is suppressed in both cases; the blockade is lifted at $V_{\mathrm{SG}} \approx 0.1 - 0.2$ V and $V_{\mathrm{LG}} \approx 0.5$ V for the SG and the LG states respectively. The threshold voltages and the current levels are approximately reproducible from device to device. (d) Differential conductance $\mathrm{d}I/\mathrm{d}V$ calculated as the numerical derivative of I in sample 1. The change in the size of the low-conductance gap is clearly observed.

the dotted rectangle is magnified in Figure 3(d). The telegraph-like switch is persistent even at low temperatures. The average lifetime of the states extracted from the plateau lengths is of the order of seconds and tenths of a second for the LG and SG states respectively. These timescales are typical of conformational switches in molecules on surfaces as observed *via* scanning tunnel microscopy.[44–46] Figure 3(c) shows a current histogram obtained from the whole data range in Figure 3(b). Two conductance states clearly emerge above the noise level in the statistics. Interestingly, the LG state centered at -0.126 nA is around 80% more stable than the SG state centered at -0.198 nA. The fit to a Lorentzian distribution gives dispersion values of 0.012 nA and 0.017 nA for the LG and SG states respectively. The narrow distributions suggest that the molecule switches back-and-forth between two distinct configurations. A similar analysis has been performed on sample 1 in Section 2 of the Supplemental Material.

Note, that the observed temperature and time dependence of the switching makes charge-offset effects an unlikely explanation for it. Charge-offsets can lead to abrupt shifts in the current but these are, however, "seen in" and "activated by" sweeping the gate voltage. In contrast, our measurements show time-dependent switching at a fixed gate voltage that can therefore not be ascribed to charge-offset effects. Furthermore, the switching rate associated with thermally-activated hoping of charges from charge trap to charge trap would be strongly temperature dependent. In contrast, we do not observe such temperature dependence of the switching in Figure 3(a). Deep traps may still be present and activated by an electrical field. However, the randomness we see in the switching rates (both in time and bias voltage) together with the reproducibility of the threshold voltages mentioned before do no support such a picture.

To analyze the plausibility of the spin-crossover scenario we have performed density functional theory (DFT) calculations of the structural and electronic properties of the Fe-SCO with the SIESTA code.[47] Quantum transport simulations of the electrical and spintronic properties of the graphene/Fe-SCO/graphene junctions were carried out with the aid of

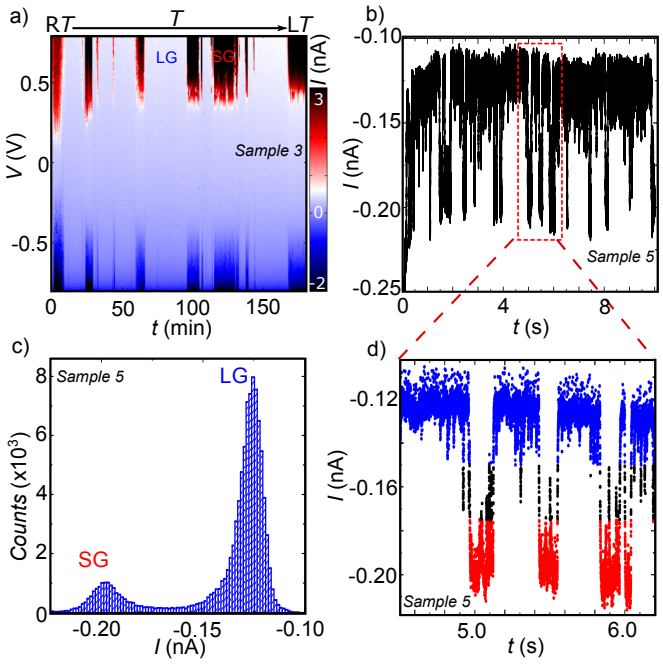

Figure 3: Temperature and time SCO stability. (a) Representative current, I, color plot as a function of the bias voltage, V, and decreasing temperature measured for sample 3. A telegraph-like switch between two well-defined bistable states occurs independently of temperature. (b) Time-trace of the current measured at a fixed V = -0.6 V and T = 2 K during 10 seconds in sample 5 (see Supplemental Material for more details of this sample). The same telegraph-like switch between two well-defined bistable states persists well below the bulk SCO transition temperature. (c) Current histogram extracted from (b). The bin size is $1.4{\cdot}10^{-3}$ nA and the total number of counts is 10^5. The LG state centered at -0.126 nA is around an 80% more stable than the SG state centered at -0.198 nA. The dispersion values taken as the full width half maximum FWHM of the fit to Lorentzian curves are 0.012 nA and 0.017 nA for the LG and the SG respectively. (d) Zoom in a reduced time scale of the current trace in (b), showing the two states clearer.

the code GOLLUM.[48,49] The simulated molecular junctions contain 2 graphene electrodes, formed by 282 C and 12 H atoms. The distance between the electrodes is set to 1.7 nm and the Fe-SCO molecule is placed bridging the electrodes so that each pyrene unit lies inside the sheets as indicated in Figure 1(b). The fully optimized molecule-electrodes structure results in a $S = 0$ (LS) ground state. A less stable $S = 2$ (HS) configuration can also be obtained, which presents larger Fe-N bonds and therefore a smaller ligand field splitting acting on the Fe(II) d orbitals. Additional details can be found in Section 3 of the Supplemental Material.

Figure 4(a) shows the spin-dependent transmission function $T_\sigma(E)$ computed for the LS and the HS states. The transmission in the LS state is spin degenerate and, at low energies, is mediated by the lowest unoccupied molecular orbital (LUMO) that lies 0.27 eV above the Fermi energy. For the HS state, the structure of $T_\sigma(E)$ around the Fermi level is remarkably different. The transmission function depends now on the spin component. The minority spin transmission function $T_\downarrow$ displays three new peaks, one of which (LUMO) is much closer (≈ 0.02 eV) to the Fermi level than in the LS state. This shift has a strong effect on the computed I-V characteristics for the HS and the LS states as shown in Figure 4(b). The calculated curves strikingly resemble to the experimental ones in Figure 2 in terms of resonant voltages (V_{LG} and V_{SG}) and current levels. By comparison, we can thus ascribe the experimental bistable conductance to a SCO transition where the SG state in the measurements corresponds to the HS state and the LG state to the LS state. This correspondence is in agreement with previous experimental reports with other SCO molecules.[14,24]

In contrast with $T_\downarrow(E)$, $T_\uparrow(E)$ is rather flat and smaller in a wide energy range. We believe that this feature could be exploited to fabricate switchable spin filters. However, for that to happen the spin direction on the molecule itself needs to be fixed for instance by introducing magnetic anisotropy. The explanation behind this spin-resolved transmission can be attributed to the different filling of the orbitals as explained in more detail in Section 3 of the Supplemental Material.

We have further analyzed the impact of the molecule's stretching on the relative energies

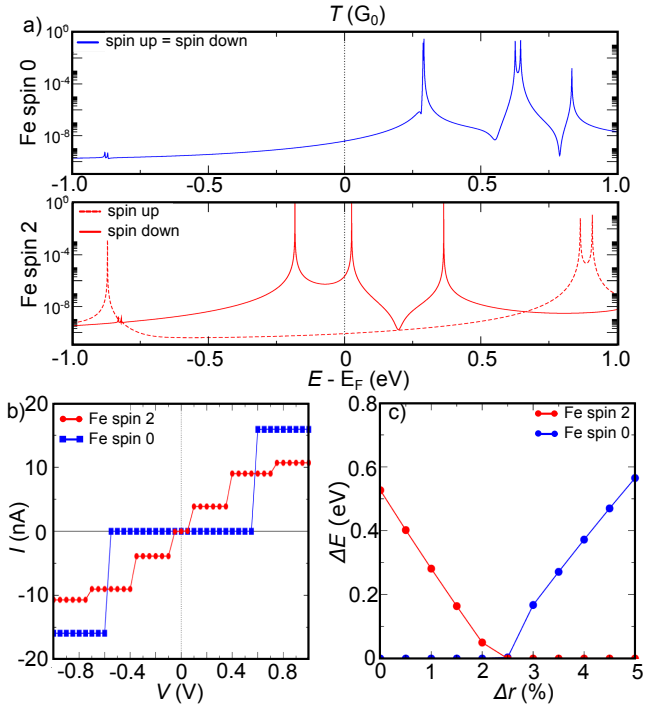

Figure 4: DFT modeling of the SCO transition. (a) Transmission as a function of energy computed for the [top] low-spin (LS) state and the [bottom] high-spin (HS) state. The SCO transition induces a strong modification of the molecular orbitals with the HS LUMO much closer to the Fermi level than the LS LUMO. In addition, the transmission in the HS state is spin resolved up to relatively high energies. (b) Current-voltage characteristics of the LS and HS states calculated from the transmission curves. The change in the level alignment is translated into a change in the current blockade gap as observed experimentally in Figure 2. (c) HS to LS energy difference ΔE relative to the lowest energy state as a function of the Fe-N bond stretching length Δr (see Supplemental Material for its definition). A small stretching Δr_c of around 2.5% can induce the spin-crossover transition form $S = 2$ to $S = 0$. Small perturbations ($< 1\%$) around that point stabilize LS or HS by more than 0.2 eV.

of its HS and LS states. However, DFT may not provide an accurate enough description of the multi-electronic state of the molecule, so we have fitted the DFT estimate of the ligand field effects for the LS state to the following multi-electronic Hamiltonian:

$$H = H_{EE} + H_{LF}, \tag{1}$$

where H_{EE} represents the electrostatic interaction between the d electrons of the Fe(II) ion and H_{LF} accounts for the ligand field interaction of the d electrons with the surrounding atoms. H_{EE} can be parametrized in terms of the Slater-Condon parameters F_k.[50] We have taken r_0 as the average distance between the central Fe(II) ion and the surrounding ligands in the most stable configuration of the molecule, and have then stretched this average distance by an amount Δr. Because the strength of the ligand field is known to be approximately proportional to r^{-5} for $3d$ electrons,[34] we have simulated the molecule's stretching by decreasing the strength of the H_{LF} term by Δr^{-5}. The total energies of the lowest LS and HS multi-electronic solutions, relative to the lowest state, are plotted in Figure 4(c). Note, that the spin transition from $S = 0$ to $S = 2$ occurs at a Δr_c as small as 2.5 %. Importantly, we note that variations of ± 1 % relative to Δr_c stabilize either of the two states by more than 0.2 eV. Translating this effect to single-molecule junctions, we expect that small perturbations to the molecule arrangement inside the gap because of bias, temperature fluctuations, vibrations, etc will trigger the spin-switching behavior even below the bulk T_c, or hinder it (as in sample 4 in the Supporting Information) depending on the junction conformation. Note that the transmission curves shown in Figure 4(a) for the LS (HS) are representative of any Δr below (above) 2.5 % with minor variations.

To further study the effect of perturbations we have displaced in the simulations the molecule perpendicular to the junction gap. We have found that the most stable configuration corresponds to the molecule's core lying inside the gap. We have also found that the molecule may drift easily inside the gap with energy barriers as small as 20 meV. However, once the core hits one of the two electrodes, the energy barrier for further drifting above

the electrode rises sharply to 0.5 - 1 eV because of steric hindrance. As a consequence, the molecule's core stays within the gap.

Long spin-state lifetimes at room temperature have been reported for SCO complexes in solution, where cooperative interactions and low-energy phonons proper of a SCO crystal are absent.[51,52] These spin transitions have been observed to involve large structural rearrangements leading to high energy barriers between the LS and HS states. Similar structural distortions have been observed for bpp derivatives.[53,54] Slow, temperature-independent SCO up to 120 K has been found in other Fe(II) complexes that share the same ligand geometry as bpp molecules.[55,56]

These two ingredients: lack of cooperative intermolecular interactions and a bpp skeleton are present in our solid-state device. The calculations (see Section 3 of the Supplemental Material) for the Fe(II) SCO molecule in this study indicate that tunneling is the dominant switching mechanism up to temperatures of the order 100 K in the absence of stimuli other than temperature, in agreement with Ref.[57] We find resident times in the range 10^{-3} - 10^{0} seconds independent of the temperature (see Section 3 of the Supplemental Material), that are consistent with our experiments. For higher temperatures vibrational heating reduces those resident times. We note here that, the temperature of a single-molecule that is voltage biased through weakly coupled electrodes is ill-defined and may be subject to fluctuations.[58]

Additionally, other stimuli, i.e. mechanical, electrical or thermal, could contribute to triggering the SCO mechanism or block it if a single-molecule is embedded in a junction. Local perturbations to the binding geometry could, for example, induce strain to the molecule ligands, which can be large enough to stretch the ligand-metal ion distance to induce the spin transition.[25] Moreover, the strong electric fields generated by the voltage in these narrow solid-state nano-junctions could induce non-equilibrium spin-orbit effects[23] or dipole-induced strain[59] in the molecule due to the opposite charge of the Fe core and the ligands. Again, these effects can influence the ligand-metal ion distance and thereby initiate the SCO transition.

In conclusion, we have measured electron transport through individual Fe-SCO molecules coupled to few-layer graphene electrodes. We observe a reproducible switching between two bistable states triggered by the SCO transition in the molecule. DFT calculations provide a qualitative and quantitative agreement thanks to the well-defined geometry of the molecule-graphene coupling. The switching occurs well below the critical temperature for crystals of the same molecules. DFT suggests that the switch at the single-molecule level can be induced by small perturbations to the ligand distance in the molecular junction. Finally, the HS state of the molecule is spin resolved; these molecules could therefore be used as switchable spin polarizers.

Acknowledgement

We acknowledge financial support from the Dutch Organization for Fundamental research (NWO/FOM), the European Commission through an advanced ERC grant (Mols@Mols) and the Marie Curie ITN MOLESCO, from the Netherlands Organization for Scientific Research (NWO/OCW) as part of the Frontiers of Nanoscience program, and from the Spanish Ministerio de Economia y Competitividad through the project FIS2015-63918-R. EB thanks funds from the EU FP7 program through Project 618082 ACMOL and NWO through a VENI fellowship.

Supporting Information Available

The following files are available free of charge.

Characterization of the empty gap, additional molecular junctions showing SCO and details of the DFT calculations.

References

(1) Bousseksou, A.; Molnár, G.; Salmon, L.; Nicolazzi, W. *Chem. Soc. Rev.* **2011**, *40*, 3313.

(2) Sanvito, S. *Chem. Soc. Rev.* **2011**, *40*, 3336–55.

(3) Lefter, C.; Davesne, V.; Salmon, L.; Molnár, G.; Demont, P.; Rotaru, A.; Bousseksou, A. *Magnetochemistry* **2016**, *2*, 18.

(4) Gütlich, P.; Garcia, Y.; Goodwin, H. A.; Murray, K. S.; Shu, J.; Hemley, R. J.; Mao, H. K.; Young, N. A.; Varret, F.; Kahn, O.; Smith, D. R.; Wieghardt, K.; Zehnder, M.; Zuberbühler, A. D. *Chem. Soc. Rev.* **2000**, *29*, 419–427.

(5) Gamez, P.; Costa, J. S.; Quesada, M.; Aromí, G. *Dalt. Trans.* **2009**, 7845–7853.

(6) Gütlich, P.; Gaspar, A. B.; Garcia, Y. *Beilstein J. Org. Chem.* **2013**, *9*, 342–391.

(7) Senthil Kumar, K.; Ruben, M. *Coord. Chem. Rev.* **2017**, *346*, 176–205.

(8) Decurtins, S.; Gutlich, P.; Hasselbach, K. M.; Hauser, A.; Spiering, H. *Inorg. Chem.* **1985**, *24*, 2174–2178.

(9) Hauser, A. *Chem. Phys. Lett.* **1986**, *124*, 543–548.

(10) Gutlich, P.; Ksenofontov, V.; Gaspar, A. *Coord. Chem. Rev.* **2005**, *249*, 1811–1829.

(11) Craig, G. A.; Costa, J. S.; Roubeau, O.; Teat, S. J.; Shepherd, H. J.; Lopes, M.; Molnár, G.; Bousseksou, A.; Aromí, G. *Dalt. Trans.* **2014**, *43*, 729–737.

(12) González-Prieto, R.; Fleury, B.; Schramm, F.; Zoppellaro, G.; Chandrasekar, R.; Fuhr, O.; Lebedkin, S.; Kappes, M.; Ruben, M. *Dalt. Trans.* **2011**, *40*, 7564.

(13) Dugay, J.; Aarts, M.; Giménez-Marqués, M.; Kozlova, T.; Zandbergen, H. W.; Coronado, E.; van der Zant, H. S. J. *Nano Lett.* **2017**, *17*, 186–193.

(14) Harzmann, G. D.; Frisenda, R.; van der Zant, H. S. J.; Mayor, M. *Angew. Chemie Int. Ed.* **2015**, *54*, 13425–13430.

(15) Li, B.; Wei, R.-J.; Tao, J.; Huang, R.-B.; Zheng, L.-S.; Zheng, Z. *J. Am. Chem. Soc.* **2010**, *132*, 1558–1566.

(16) Coronado, E.; Giménez-Marqués, M.; Mínguez Espallargas, G.; Rey, F.; Vitórica-Yrezábal, I. J. *J. Am. Chem. Soc.* **2013**, *135*, 15986–15989.

(17) Sánchez-Costa, J.; Rodríguez-Jiménez, S.; Craig, G. A.; Barth, B.; Beavers, C. M.; Teat, S. J.; Aromí, G. *J. Am. Chem. Soc.* **2014**, *136*, 3869–3874.

(18) Prins, F.; Monrabal-Capilla, M.; Osorio, E. A.; Coronado, E.; van der Zant, H. S. J. *Adv. Mater.* **2011**, *23*, 1545–9.

(19) Lefter, C.; Rat, S.; Costa, J. S.; Manrique-Juárez, M. D.; Quintero, C. M.; Salmon, L.; Séguy, I.; Leichle, T.; Nicu, L.; Demont, P.; Rotaru, A.; Molnár, G.; Bousseksou, A. *Adv. Mater.* **2016**, *28*, 7508–7514.

(20) Miyamachi, T.; Gruber, M.; Davesne, V.; Bowen, M.; Boukari, S.; Joly, L.; Scheurer, F.; Rogez, G.; Yamada, T. K.; Ohresser, P.; Beaurepaire, E.; Wulfhekel, W. *Nat. Commun.* **2012**, *3*, 938.

(21) Bedoui, S.; Molnár, G.; Bonnet, S.; Quintero, C.; Shepherd, H. J.; Nicolazzi, W.; Salmon, L.; Bousseksou, A. *Chem. Phys. Lett.* **2010**, *499*, 94–99.

(22) Bertoni, R.; Lorenc, M.; Cailleau, H.; Tissot, A.; Laisney, J.; Boillot, M.-L.; Stoleriu, L.; Stancu, A.; Enachescu, C.; Collet, E. *Nat. Mater.* **2016**, *15*, 606–610.

(23) Meded, V.; Bagrets, A.; Fink, K.; Chandrasekar, R.; Ruben, M.; Evers, F.; Bernand-Mantel, A.; Seldenthuis, J. S.; Beukman, A.; van der Zant, H. S. J. *Phys. Rev. B* **2011**, *83*, 245415.

(24) Frisenda, R.; Harzmann, G. D.; Celis Gil, J. A.; Thijssen, J. M.; Mayor, M.; van der Zant, H. S. J. *Nano Lett.* **2016**, *16*, 4733–4737.

(25) Kuang, G.; Zhang, Q.; Lin, T.; Pang, R.; Shi, X.; Xu, H.; Lin, N. *ACS Nano* **2017**, *11*, 6295–6300.

(26) Heersche, H. B.; de Groot, Z.; Folk, J. A.; van der Zant, H. S. J.; Romeike, C.; Wegewijs, M. R.; Zobbi, L.; Barreca, D.; Tondello, E.; Cornia, A. *Phys. Rev. Lett.* **2006**, *96*, 206801.

(27) Gaudenzi, R.; Burzurí, E.; Reta, D.; Moreira, I. d. P. R.; Bromley, S. T.; Rovira, C.; Veciana, J.; van der Zant, H. S. J. *Nano Lett.* **2016**, *16*, 2066–2071.

(28) Burgess, J. A. J.; Malavolti, L.; Lanzilotto, V.; Mannini, M.; Yan, S.; Ninova, S.; Totti, F.; Rolf-Pissarczyk, S.; Cornia, A.; Sessoli, R.; Loth, S. *Nat. Commun.* **2015**, *6*, 8216.

(29) Burzurí, E.; Gaudenzi, R.; van der Zant, H. S. J. *J. Phys. Condens. Matter* **2015**, *27*, 113202.

(30) Warner, B.; Oberg, J. C.; Gill, T. G.; El Hallak, F.; Hirjibehedin, C. F.; Serri, M.; Heutz, S.; Arrio, M.-A.; Sainctavit, P.; Mannini, M.; Poneti, G.; Sessoli, R.; Rosa, P. *J. Phys. Chem. Lett.* **2013**, *4*, 1546–1552.

(31) Burzurí, E.; Prins, F.; Van Der Zant, H. S. J. *Graphene* **2012**, *1*, 26–29.

(32) García-Suárez, V. M.; Ferradás, R.; Carrascal, D.; Ferrer, J. *Phys. Rev. B* **2013**, *87*, 235425.

(33) Bernien, M.; Naggert, H.; Arruda, L. M.; Kipgen, L.; Nickel, F.; Miguel, J.; Hermanns, C. F.; Krüger, A.; Krüger, D.; Schierle, E.; Weschke, E.; Tuczek, F.; Kuch, W. *ACS Nano* **2015**, *9*, 8960–8966.

(34) Newman, D. J.; Ng, B. K. C. *Crystal Field Handbook*; Cambridge University Press, 2000.

(35) Prins, F.; Barreiro, A.; Ruitenberg, J. W.; Seldenthuis, J. S.; Aliaga-Alcalde, N.; Vandersypen, L. M. K.; van der Zant, H. S. J. *Nano Lett.* **2011**, *11*, 4607–4611.

(36) Island, J. O.; Holovchenko, A.; Koole, M.; Alkemade, P. F. A.; Menelaou, M.; Aliaga-Alcalde, N.; Burzurí, E.; van der Zant, H. S. J. *J. Phys. Condens. Matter* **2014**, *26*, 474205.

(37) Burzurí, E.; Island, J. O.; Díaz-Torres, R.; Fursina, A.; González-Campo, A.; Roubeau, O.; Teat, S. J.; Aliaga-Alcalde, N.; Ruiz, E.; van der Zant, H. S. J. *ACS Nano* **2016**, *10*, 2521–2527.

(38) Perrin, M. L.; Burzurí, E.; van der Zant, H. S. J. *Chem. Soc. Rev.* **2015**, *44*, 902–19.

(39) Carrascal, D.; García-Suárez, V. M.; Ferrer, J. *Phys. Rev. B* **2012**, *85*, 195434.

(40) Ullmann, K.; Coto, P. B.; Leitherer, S.; Molina Ontoria, A.; Martín, N.; Thoss, M.; Weber, H. B. *Nano Lett.* **2015**, *15*, 3512–3518.

(41) Mol, J. A.; Lau, C. S.; Lewis, W. J. M.; Sadeghi, H.; Roche, C.; Cnossen, A.; Warner, J. H.; Lambert, C. J.; Anderson, H. L.; Briggs, G. A. D. *Nanoscale* **2015**, *7*, 13181–13185.

(42) Lumetti, S.; Candini, A.; Godfrin, C.; Balestro, F.; Wernsdorfer, W.; Klyatskaya, S.; Ruben, M.; Affronte, M. *Dalt. Trans.* **2016**, *45*, 16570–16574.

(43) Sarwat, S. G.; Gehring, P.; Rodriguez Hernandez, G.; Warner, J. H.; Briggs, G. A. D.; Mol, J. A.; Bhaskaran, H. *Nano Lett.* **2017**, *17*, 3688–3693.

(44) Liljeroth, P.; Repp, J.; Meyer, G. *Science* **2007**, *317*, 1203–1206.

(45) Komeda, T.; Isshiki, H.; Liu, J.; Zhang, Y.-F.; Lorente, N.; Katoh, K.; Breedlove, B. K.; Yamashita, M. *Nat. Commun.* **2011**, *2*, 217.

(46) Zhang, J. L.; Zhong, J. Q.; Lin, J. D.; Hu, W. P.; Wu, K.; Xu, G. Q.; Wee, A. T. S.; Chen, W. *Chem. Soc. Rev.* **2015**, *44*, 2998–3022.

(47) Soler, J. M.; Artacho, E.; Gale, J. D.; García, A.; Junquera, J.; Ordejón, P.; Sánchez-Portal, D. *J. Phys. Condens. Matter* **2002**, *14*, 2745–2779.

(48) Ferrer, J.; Lambert, C. J.; García-Suárez, V. M.; Manrique, D. Z.; Visontai, D.; Oroszlany, L.; Rodríguez-Ferradás, R.; Grace, I.; Bailey, S. W. D.; Gillemot, K.; Sadeghi, H.; Algharagholy, L. A. *New J. Phys.* **2014**, *16*, 093029.

(49) García-Suárez, V. M.; Ferrer, J. *Phys. Rev. B* **2012**, *86*, 125446.

(50) Griffith, J. S. J. S. *The theory of transition-metal ions.*; University Press, 1971; p 455.

(51) Stock, P.; Pędziński, T.; Spintig, N.; Grohmann, A.; Hörner, G. *Chem. - A Eur. J.* **2013**, *19*, 839–842.

(52) Stock, P.; Deck, E.; Hohnstein, S.; Korzekwa, J.; Meyer, K.; Heinemann, F. W.; Breher, F.; Hörner, G. *Inorg. Chem.* **2016**, *55*, 5254–5265.

(53) Kershaw Cook, L. J.; Thorp-Greenwood, F. L.; Comyn, T. P.; Cespedes, O.; Chastanet, G.; Halcrow, M. A. *Inorg. Chem.* **2015**, *54*, 6319–6330.

(54) Zhang, X.; Lawson Daku, M. L.; Zhang, J.; Suarez-Alcantara, K.; Jennings, G.; Kurtz, C. A.; Canton, S. E. *J. Phys. Chem. C* **2015**, *119*, 3312–3321.

(55) Renz, F.; Oshio, H.; Ksenofontov, V.; Waldeck, M.; Spiering, H.; Gütlich, P. *Angew. Chemie* **2000**, *39*, 3699–3700.

(56) Hauser, A.; Enachescu, C.; Daku, M. L.; Vargas, A.; Amstutz, N. *Coord. Chem. Rev.* **2006**, *250*, 1642–1652.

(57) Xie, C. L.; Hendrickson, D. N. *J. Am. Chem. Soc.* **1987**, *109*, 6981–6988.

(58) Ward, D. R.; Corley, D. A.; Tour, J. M.; Natelson, D. *Nat. Nanotechnol.* **2011**, *6*, 33–38.

(59) Weston, L.; Cui, X.; Ringer, S.; Stampfl, C. *Phys. Rev. Lett.* **2015**, *114*, 247601.